A Generalized Method for Estimating the Structure of the Equatorial Atlantic Cold Tongue: Application to Drifter Observations

VERENA HORMANN*

Cooperative Institute for Marine and Atmospheric Studies, University of Miami, and NOAA/Atlantic Oceanographic and Meteorological Laboratory, Miami, Florida

RICK LUMPKIN

NOAA/Atlantic Oceanographic and Meteorological Laboratory, Miami, Florida

RENELLYS C. PEREZ

Cooperative Institute for Marine and Atmospheric Studies, University of Miami, and NOAA/Atlantic Oceanographic and Meteorological Laboratory, Miami, Florida

(Manuscript received 17 August 2012, in final form 8 February 2013)

ABSTRACT

A generalized method is developed to determine the position of the Atlantic northern cold tongue front across its zonal extent from satellite sea surface temperature (SST) data. Previous approaches estimated the frontal position subjectively or individually, calling for a more objective technique that is suitable for large datasets. The developed methodology is based on a median frontal SST, and associated positional uncertainties are on the order of 0.3° latitude for the period 1998–2011. Frontal characteristics are generally consistent with tropical instability waves (TIWs) and interannual variations are large. Application to drifter observations shows how the new methodology can be used to better understand circulation features near the northern cold tongue front. A drifter pair deployed on the eastern side of a passing TIW crest north of the front revealed that the trajectories of the drifters were clearly influenced by the shape of the front and they did not cross the front, but rather stayed close together about 2.5° north of the front. In a more complete analysis using all available drifters near the Atlantic northern cold tongue front, only about 12% of the trajectories crossed the front. Analyses in an along- and cross-frontal frame of reference complement isopycnal coordinate mapping, and tropical Atlantic drifter velocities averaged in frontal coordinates indicate a broadened shear zone between the northern branch of the South Equatorial Current and North Equatorial Countercurrent as well as meridional convergence near the front.

1. Introduction

In the central and eastern tropical Atlantic, a pronounced sea surface temperature (SST) front develops north of the equator during boreal summer and fall (Fig. 1a) coincident with the onset of the cold tongue (e.g., Legeckis and Reverdin 1987; Steger and Carton 1991). This temperature front separates the cold equatorial waters from the warmer northern ones and forms the boundary between the northern branch of the westward-flowing South Equatorial Current (nSEC) and the eastward-flowing North Equatorial Countercurrent (NECC). The front exhibits large undulations because of tropical instability waves (TIWs; e.g., Düing et al. 1975; Legeckis and Reverdin 1987; Steger and Carton 1991), westward-propagating phenomena believed to be generated by barotropic and baroclinic instabilities associated with the meridional and vertical shear of the equatorial zonal current system (e.g., Philander 1978; Weisberg and Weingartner 1988; Grodsky et al. 2005). TIWs are also associated with anticyclonic tropical instability vortices (TIVs) north of the front that involve a complex

* Current affiliation: Scripps Institution of Oceanography, University of California, San Diego, La Jolla, California.

Corresponding author address: Verena Hormann, Scripps Institution of Oceanography, University of California, San Diego, 9500 Gilman Drive, Mail Code 0213, La Jolla, CA 92093.
E-mail: vhormann@ucsd.edu

DOI: 10.1175/JTECH-D-12-00173.1

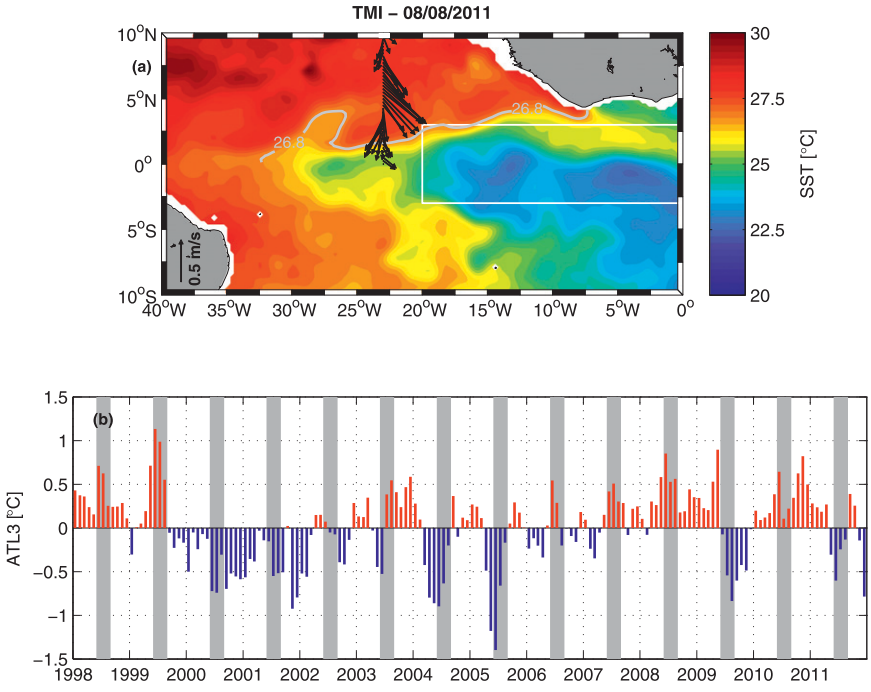

FIG. 1. (a) TMI SST in the equatorial Atlantic on 8 Aug 2011, with concurrent 30-m ADCP currents from the PNE11 cruise along 23°W superimposed (black vectors, scale indicated in the figure) and 26.8°C isotherm (gray) indicating the isotherm associated with the northern cold tongue front as inferred from PNE11-XBT data via the maximum 1-m temperature gradient (cf. Fig. 2); note the uniformly southward near-surface currents associated with the eastern side of a passing TIW crest. The white box in (a) defines the region for the ATL3 SST index (Zebiak 1993) shown in (b), where monthly area-averaged anomalies were calculated by subtracting the mean seasonal cycle; gray shadings highlight boreal summer.

three-dimensional circulation from the surface down to the thermocline (e.g., Steger and Carton 1991; Kennan and Flament 2000; Menkes et al. 2002; Foltz et al. 2004). Their activity can vary dramatically from one year to the next (e.g., Steger and Carton 1991; Caltabiano et al. 2005; Wu and Bowman 2007a; Perez et al. 2012) and lead to interannual variations in the atmospheric response (e.g., Caltabiano et al. 2005; Wu and Bowman 2007b). Moreover, TIWs are thought to play a key role in the equatorial cold tongue heat balance (e.g., Hansen and Paul 1984; Weisberg and Weingartner 1988; Foltz et al. 2003; Jochum et al. 2004), and to affect marine biogeochemistry (e.g., Menkes et al. 2002; Evans et al. 2009) and upper-ocean salinity (Grodsky et al. 2005; Lee et al. 2012).

The sharp temperature gradient associated with the northern cold tongue front implies that northward-moving cold water on the southern side cannot directly cross the front, leading to a slantwise motion at the front as described in both Atlantic and Pacific model studies (Dutrieux et al. 2008; Perez et al. 2010). Dutrieux et al. (2008) showed that particles do eventually cross the front and that TIVs play a key role in such crossings. They further found profound differences between an experiment where floats were forced to remain at the surface and a three-dimensional experiment: In the two-dimensional experiment, particles tended to concentrate in convergence zones such as along the shear zone between the nSEC and NECC, while in the three-dimensional experiment the particles stayed more homogeneously distributed and better sampled the TIVs.

Because of the importance of frontal processes such as those associated with TIWs and the related TIVs, it is essential to estimate the structure of the equatorial Atlantic cold tongue in a frontal coordinate system defined by the position of the front. Previous studies derived the frontal position subjectively or individually (Legeckis and Reverdin 1987; Steger and Carton 1991; Johnson 1996; Perez et al. 2010). The approach by Steger and Carton (1991), for instance, was based on hand-drawn SST analyses and their estimates of the Atlantic cold tongue front followed approximately the 25° or 27°C isotherm, but these results are specific to the time period of their study. More recently, Perez et al. (2010) used the latitude of the largest meridional near-surface temperature gradient, located between the cold tongue minimum and the edge of the northern Pacific cold tongue front, to individually

identify the front in 38 shipboard acoustic Doppler current profiler (ADCP) latitude–depth sections. This methodology, however, was not designed to handle the complex structure of the front across its whole zonal extent nor was it intended to be applied to large datasets.

Interannual variability in the central and eastern equatorial Atlantic is large (Fig. 1b) and the characteristics of the cold tongue vary from year to year. Therefore, there is a clear need for an improved, rigorous, and generalized frontal detection technique that is suitable for application to large datasets across multiple seasons. The goal of this study is to develop such a generalized method (section 3) that can be used to study and better understand circulation features along the northern front. To validate the methodology and demonstrate its value, the new methodology will be applied to observations from near-surface satellite-tracked drifting buoys (hereafter ''drifters'') in the tropical Atlantic (section 4). The data are described in section 2, and discussion and conclusions are provided in section 5.

2. Data

The methodology is based on gridded SSTs from the Tropical Rainfall Measuring Mission (TRMM) Microwave Imager (TMI) as provided by Remote Sensing Systems (http://www.remss.com/). Version 4 TMI data are globally available between 40°S and 40°N at a spatial resolution of 0.25° as daily 3-day averages from December 1997 onward, with SST fields slightly smoothed by a Gaussian interpolation scheme (influence and cutoff radii of 0.25° and 0.5°, respectively) to fill remaining gaps. An in situ validation of TMI SSTs by Gentemann et al. (2004) revealed a mean bias of −0.07°C and a standard deviation of 0.57°C in comparison to moored observations in the tropical Pacific and Atlantic; their suitability within the scope of Atlantic TIW studies has been widely demonstrated (e.g., Caltabiano et al. 2005; Grodsky et al. 2005; Wu and Bowman 2007a; Perez et al. 2012).

As a first application of the frontal dataset, we use observations from drogued near-surface drifters of the Global Drifter Program (GDP; Niiler 2001; Lumpkin and Pazos 2007), which have been subject to the systematic manual reevaluation of drogue presence after Lumpkin et al. (2013), to study the near-frontal circulation in the tropical Atlantic. Drifter-derived observations of horizontal velocity at the drogue depth of 15 m and temperatures at 20–30-cm depth were quality controlled (Hansen and Poulain 1996) and are available at regular 6-h intervals. In particular, we examine new Lagrangian observations from a drifter pair deployed north of the cold tongue front at 3°21.37′N, 22°59.197′W on 8 August 2011 during the Prediction and Research Moored Array in the Tropical Atlantic (PIRATA) Northeast Extension 2011 (PNE11) cruise. Drifter 92982 and drifter 106556 stopped transmitting on 9 October 2011 and 15 September 2011, respectively; the unusually short lifetime of both drifters was found to be related to leaking battery packs. Using expendable bathythermograph (XBT) data collected during the PNE11 cruise, the quasi-synoptic frontal position was estimated as 1.6°N via the maximum 1-m temperature gradient, which is in close agreement with the front position at 1.4°N derived from the maximum gradient of TMI SST along the cruise track (Fig. 2), a defining feature of the frontal position used in one step of the new methodology. Later in this study, we apply the methodology to examine the behavior of all GDP drifters in our study region.

3. Methodology

A major feature of the tropical Atlantic variability is the seasonal appearance of a cold tongue in the central and eastern equatorial basin. The cold tongue temperature shows large interannual variations as typically expressed by the ATL3 SST index, or the area-averaged SST anomaly in the region 3°S–3°N, 20°W–0° (Zebiak 1993; Fig. 1b), and thus the timing of the cold tongue onset and termination can also vary from year to year. Studying intraseasonal to interannual modulations of the cold tongue structure therefore requires objective criteria for its onset and termination: Brandt et al. (2011) defined the cold tongue onset as the date when the surface area where the SST is colder than 25°C within the region 5°S–5°N, 30°W–12°E exceeds the empirically fixed threshold of $0.4 \times 10^6\,\mathrm{km}^2$. However, for their application Brandt et al. (2011) did not need to determine its termination. Inspection of the temporal evolution of this surface area bounded by the 25°C isotherm and corresponding area-averaged SSTs led us to set the termination of the cold tongue as the date when that surface area falls below 50% of its maximum extent, that is, taking different manifestations into account as illustrated in Fig. 3 for extremes of the ATL3 SST index (cf. Fig. 1b).

Our new methodology to locate the northern cold tongue front is as follows:

1) Calculations are limited to the yearly cold tongue duration using the onset and termination criteria defined above for the full TMI SST record 1998–2011 (Table 1).
2) At each time step, the latitude of the largest (absolute) meridional SST gradient, $\varphi_{\mathrm{grad}}\,(t, x)$, is calculated between 3°S and 6°N for all longitudes within the range 30°W–5°E (i.e., including the ATL3 cold tongue region) and the SST at each φ_{grad}, $\mathrm{SST}_{\mathrm{grad}}\,(t, x)$, is determined.

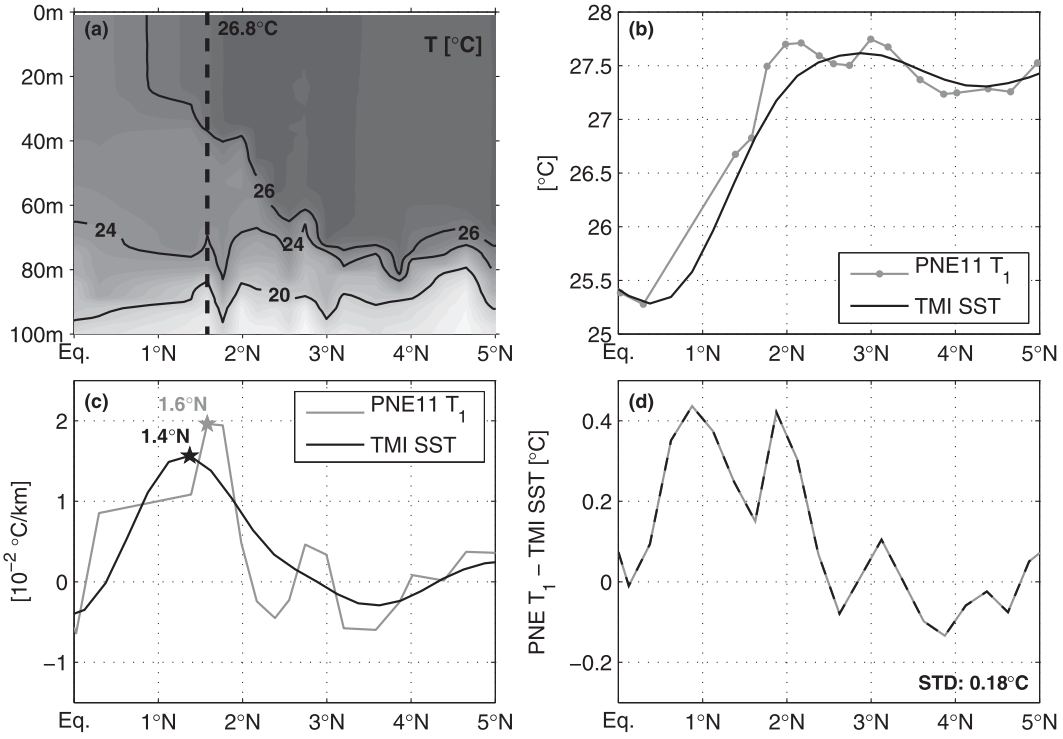

FIG. 2. (a) Temperature distribution from PNE11-XBT data along 23°W; dashed line marks position of the northern cold tongue front at 1.6°N, corresponding to the maximum temperature gradient at 1-m depth [gray star in (c)]. (b)–(d) Comparison of PNE11-XBT 1-m temperatures [gray, points in (b) mark XBT drop locations] and TMI SSTs (black); standard deviation of their difference (gray − black) is annotated in (d).

3) Finally, the isotherm of the median SST_{grad} for all longitudes, $\langle SST_{grad} \rangle$ (t), is used to identify the latitudinal position of the cold tongue front in the region 30°W–5°E at each time step.

This method combines features of the front used in prior studies (Legeckis and Reverdin 1987; Steger and Carton 1991; Johnson 1996; Perez et al. 2010): the strong meridional temperature gradient associated with the front, and the observed characteristic that the front can be delineated by a fixed isotherm at a given time. Unlike more traditional meridional gradient methods such as described by Perez et al. (2010) for individual ship transects along specific longitudes, this new methodology based on $\langle SST_{grad} \rangle$ removes spurious east–west discontinuities along the zonal extent of the northern cold tongue front. Such discontinuities can result from TIW cusps, which perturb the shape of the front as they propagate westward, or effects at the western and eastern edges of the cold tongue, where the SST gradients at the front may be weaker. Figure 4 shows a comparison between our generalized method and the methodology of Perez et al. (2010) for 23° and 10°W during boreal summer. As expected, the agreement between the two methods is much larger in the core of the cold tongue, where SST gradients are strongest than closer to its western edge (correlations of 0.87 and 0.81 at 10°W vs 0.43 and 0.51 at 23°W in July and August, respectively).

Uncertainties associated with $\langle SST_{grad} \rangle$ can be estimated by a nonparametric bootstrap approach by generating random resamples from SST_{grad} at each time step and determining the corresponding median frontal SST; a thousand such realizations for each time step provide a distribution of the frontal SST that allows us to obtain 95% confidence intervals using the bias-corrected and accelerated percentile method (Efron 1987). Based on yearly cold tongue averages (Table 1), the overall mean position of the northern front is found at about 0.8°N for the period 1998–2011 and the corresponding overall positional uncertainty associated with $\langle SST_{grad} \rangle$ is on the order of 0.3° latitude. This error estimate agrees well with Legeckis and Reverdin (1987), while Steger and Carton (1991) noted positional errors of the front to be less than 0.2° latitude with their subjective methodology.

Figure 5 shows the July- and August-mean frontal SSTs and positions within the common zonal extent of the cold tongue for all years 1998–2011 in the longitude

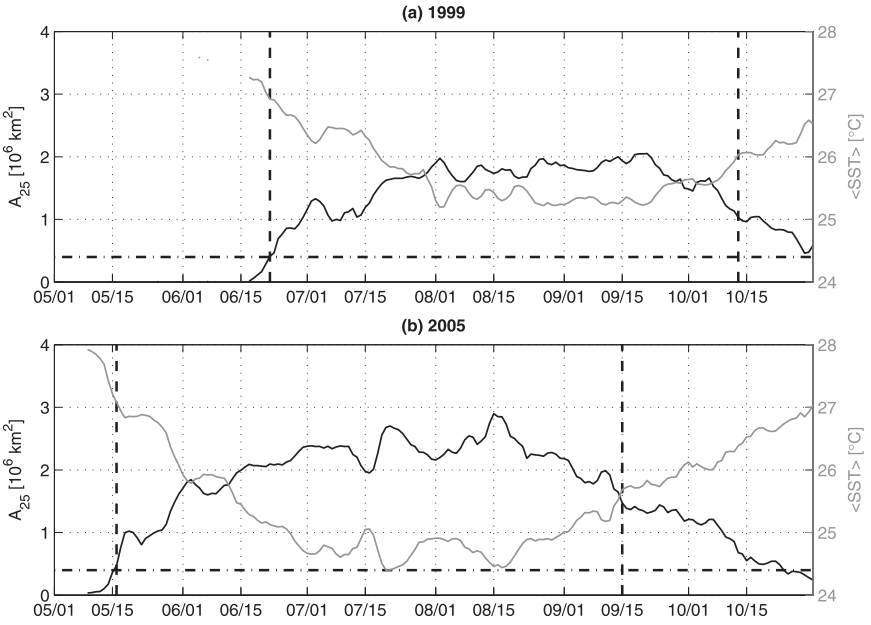

FIG. 3. Development of the surface area (black) where the SST is below 25°C within the region 5°S–5°N, 30°W–12°E and corresponding mean SST (gray) for the overall region during May–October, for the boreal summer ATL3 (a) maximum in 1999 and (b) minimum in 2005 (cf. Fig. 1b); dashed–dotted line defines the empirically fixed threshold of 0.4×10^6 km^2 by Brandt et al. (2011), and dashed lines mark onset and termination dates of the cold tongue (see section 3 for details).

range 19°–6°W (Table 1), along with corresponding uncertainties. The front is generally located farther south in August than in July (mean, with standard deviation: 0.8 ± 0.2°N and 1.4 ± 0.4°N, respectively), and the correlation between the frontal positions in these 2 months is 0.75 (Fig. 5b). During years of higher TIW variability in the latitudinal band 1°–3°N, 25°W–0° (after Perez et al. 2012; Table 1 and Fig. 5c), the front also

TABLE 1. Frontal characteristics for the full TMI SST record along with corresponding seasonal peak 4-month TIW variance averaged over the latitudinal band 1°–3°N, 25°W–0° (after Perez et al. 2012). Time period is defined as Atlantic cold tongue duration (cf. section 3), and the longitude range refers to the common zonal extent of the cold tongue during this period (i.e., full data coverage). Mean latitudinal position, westward phase speed, and average periodicity of the front are given for the common time and space scales of all years: July–August, 19°–6°W; corresponding means are annotated below. Averaging over each year's full cold tongue duration and extent yields an overall mean frontal position at about 0.8°N (cf. section 3).

Year	Time period	Lon range	Mean lat position (°N)	Phase speed (m s^{-1})	Average periodicity (day)	TIW variance (°C^2)
1998	17 Jun–23 Sep	20.25°W–5.00°E	1.1	−0.38	37	0.032
1999	22 Jun–13 Oct	20.50°W–5.00°E	0.9	−0.41	30	0.026
2000	31 May–16 Sep	24.00°W–5.00°E	2.1	−0.21	46	0.039
2001	4 Jun–29 Sep	23.50°–3.25°W	1.6	−0.43	40	0.050
2002	10 Jun–10 Oct	23.00°W–5.00°E	1.4	−0.28	42	0.037
2003	30 May–16 Sep	24.25°–5.25°W	1.3	−0.17	47	0.032
2004	18 May–13 Sep	20.50°–1.50°W	1.4	−0.34	30	0.041
2005	16 May–15 Sep	22.50°–1.50°W	1.7	−0.36	38	0.046
2006	21 Jun–26 Sep	24.00°W–0.75°E	1.5	−0.32	46	0.024
2007	14 Jun–14 Sep	24.00°W–5.00°E	0.8	−0.51	30	0.025
2008	20 Jun–28 Sep	22.50°W–5.00°E	1.2	−0.50	26	0.028
2009	7 Jun–1 Oct	23.75°–2.75°W	2.0	−0.37	38	0.049
2010	11 Jun–29 Sep	19.75°W–5.00°E	1.5	−0.05	34	0.034
2011	29 May–21 Sep	22.00°–1.50°W	1.9	−0.25	47	0.037
			1.5	−0.33 Means	38	

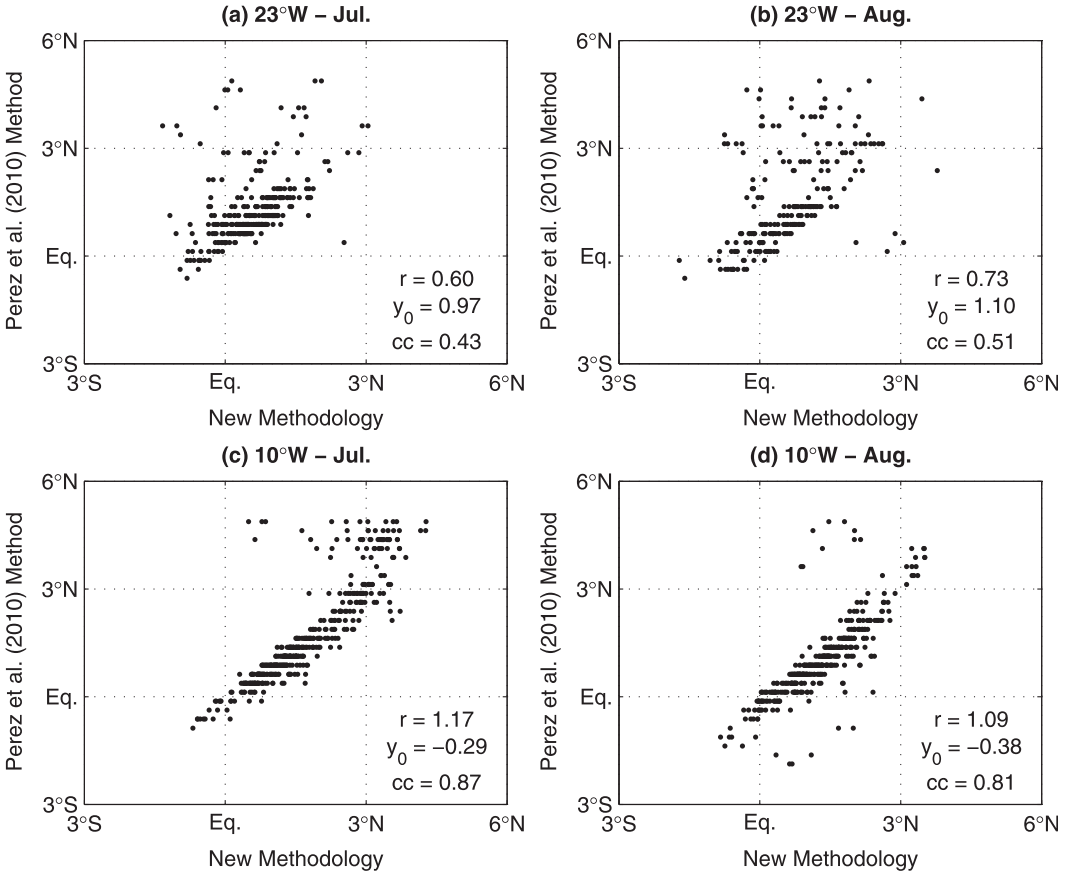

FIG. 4. Comparison between the new methodology (horizontal axes) and the methodology of Perez et al. (2010) (vertical axes) at (a),(b) 23° and (c),(d) 10°W for the months of (left) July and (right) August; corresponding regression [r, y_0] and correlation coefficients (cc) are annotated—all significant at the 95% confidence level.

appears to be farther from the equator (correlations of 0.68 and 0.40 for July and August, respectively) and frontal SSTs tend to be cooler (correlations of −0.79 and −0.51 for July and August, respectively). To further illustrate variations between years of different TIW activity, detrended frontal position anomalies are mapped onto a regular longitude–time grid using a Gaussian interpolation scheme (influence and cutoff radii of 0.5° and 1° as well as 2 and 4 days, respectively). Figure 6 shows the distributions for more moderate TIW years 1998 and 2011 as well as for the record maximum and minimum TIW years 2001 and 2006, respectively (cf. Perez et al. 2012), and highlights the large interannual variations of the front associated with TIWs. In particular, the positive and negative frontal position anomalies appear to be smaller (larger) during weaker (moderate and strong) TIW years. Similar to Steger and Carton (1991), we also determined the zonal phase speed of the temperature front from the detrended position anomalies using a Radon transform (e.g., Deans 1983) and found westward propagation speeds with magnitudes between 0.05 and 0.51 m s^{-1} within the common longitude range 19°–6°W during July–August (cf. Fig. 6; Table 1). These values are consistent with westward-propagating TIWs that have typical phase speeds between 0.1 and 0.6 m s^{-1} (e.g., Qiao and Weisberg 1995), and the same holds for the corresponding average periodicities, which have here been estimated from the maximum variance explained by least squares fits to single harmonics (Table 1). Considerably different propagation speeds for comparable periods, such as in 2001 and 2011, may be explained by widely differing prevailing TIW wavelengths (cf. Qiao and Weisberg 1995, their Table 1).

4. Application to drifter observations

Shipboard ADCP measurements (Fig. 1a) and near-real-time output of the operational numerical forecasting system at Mercator Ocean (Drévillon et al. 2008) indicated that the PNE11 cruise along 23°W would be transiting through the eastern side (or trailing edge) of a TIW crest on 8 August 2011, providing the unique

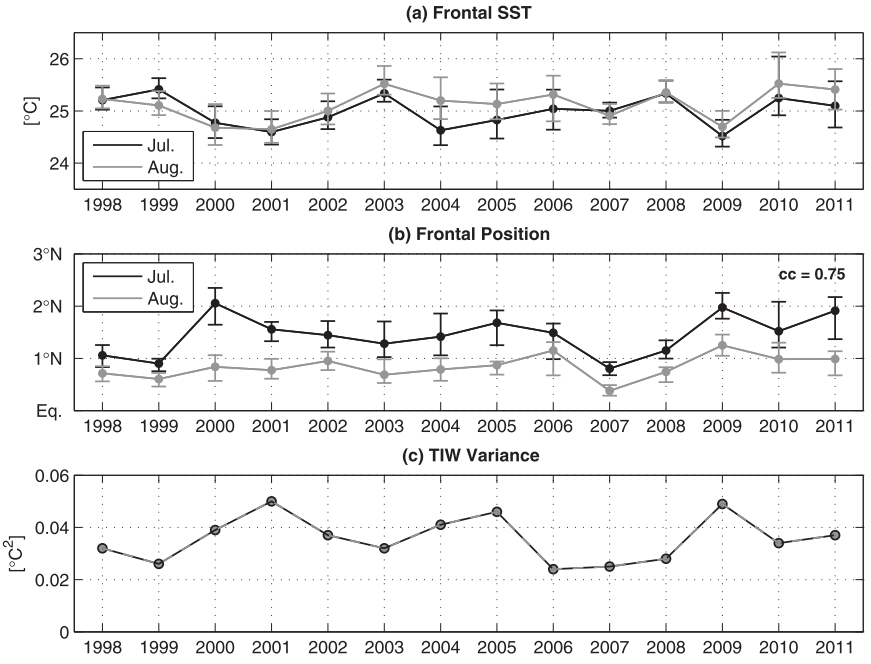

FIG. 5. Mean frontal (a) SST and (b) position within the common longitude range 19°–6°W for the months of July (black) and August (gray), with corresponding uncertainty estimates; the correlation coefficient (cc) between the frontal positions in July and August is annotated on (b). (c) Seasonal peak TIW variance in the latitudinal band 1°–3°N, 25°W–0° (after Perez et al. 2012; cf. Table 1).

opportunity to study the behavior of a drifter pair deployed near the northern cold tongue front in the presence of a TIW. Although drifter trajectories in the Atlantic cold tongue south of the equator have already been noted to be influenced by TIWs (Legeckis and Reverdin 1987) and drifters have previously been used in the description of the associated TIVs (e.g., Kennan and Flament 2000; Menkes et al. 2002; Foltz et al. 2004), their evaluation close to the actual position of the westward-propagating northern cold tongue front is still lacking. Data collected from drifters, which can be regarded as quasi-Lagrangian particles, also provide a means to examine the permeability of the front from an observational perspective using the new methodology. We first discuss in detail the PNE11 drifter pair (Fig. 7) and then put these observations in a broader context by utilizing the trajectories of all drogued drifters within the tropical Atlantic region 10°S–10°N, 30°W–5°E in the presence of the northern cold tongue front (Fig. 8).

The PNE11 drifter pair propagated mainly westward (Figs. 7b,c) and stayed close together, with maximum separation distances of about 20 km (Fig. 7a). At first glance the trajectories appear to be cycloids, but they do not transform to closed ellipses in a translating frame of reference (not shown) as typically found for drifters trapped in TIVs. The nonlooping and noncycloidal trajectories of the drifter pair rather exhibited meridional meanders governed by the location of the northern cold tongue front: Both drifters generally followed the movements of the front and maintained a latitudinal position about 2.5° north of the front (Figs. 7b,c). As the drifters propagated westward, their separation distance grew (shrank) when they were decelerating (accelerating) while moving northward (southward). At the western edge of the cold tongue, the still-transmitting drifter 92982 accelerated significantly, to a speed almost twice as fast as it had exhibited east of 30°W (Fig. 7b). This initially zonal acceleration suggests that the drifter had entered the nSEC. Toward the end of its lifetime, the drifter moved from close to the equator to about 2°N associated with a decrease in its speed west of about 34°W, suggesting that the drifter had moved north of the nSEC core. The overall behavior of the drifters with respect to the northern cold tongue front is also confirmed by a corresponding analysis using SSTs measured by the drifters along with the frontal SSTs (not shown).

To further demonstrate the usefulness of our new methodology, we now analyze the trajectories of all drifters near the Atlantic northern cold tongue front for the period 1998–2011 when the cold tongue is present (Fig. 8a). Out of the available 352 drifters, only 43 trajectories (~12%; 19 drifters were deployed in the ATL3 cold tongue region) crossed the front in the longitude

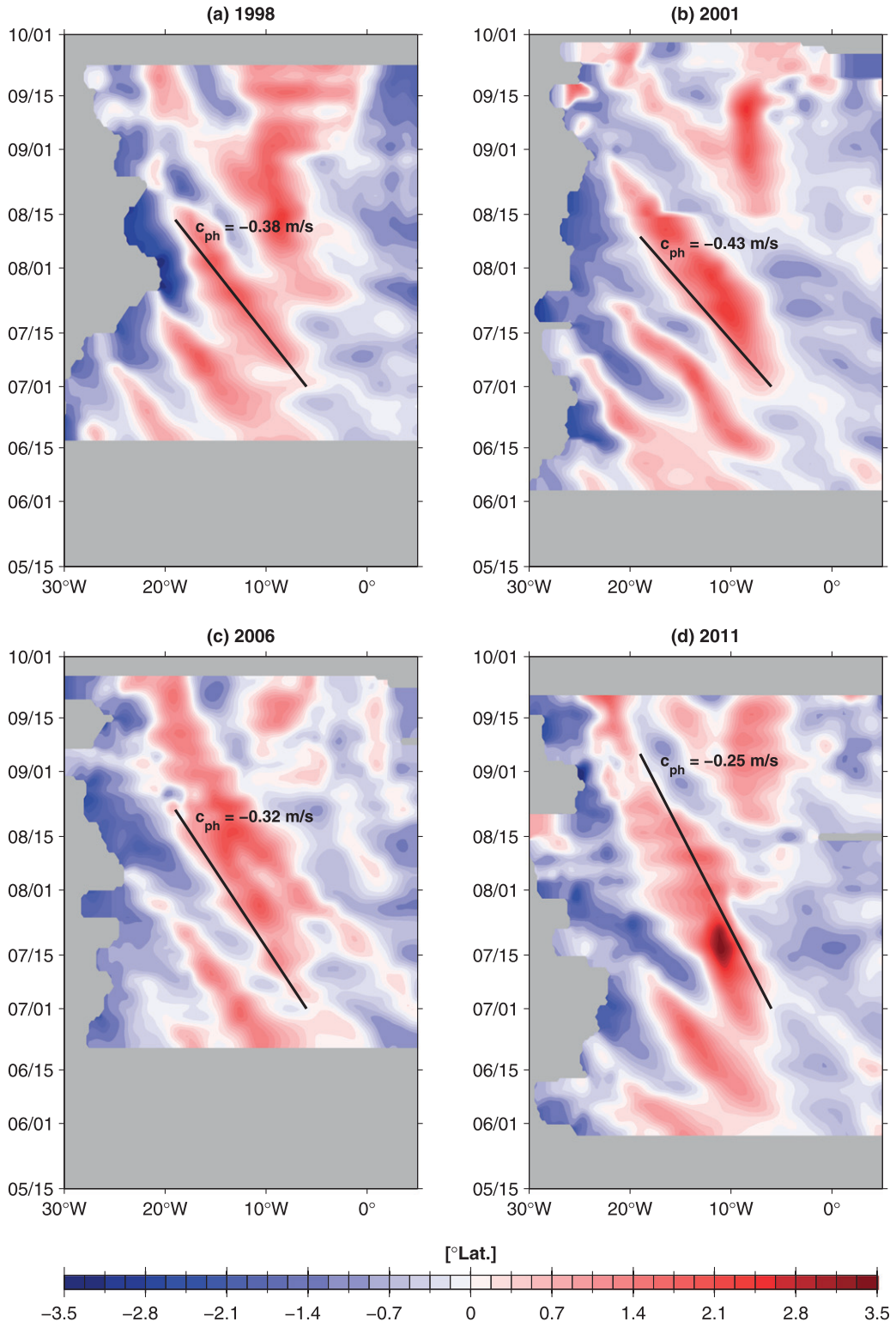

FIG. 6. Gridded frontal position anomalies (a linear trend has been removed before mapping) between 30°W and 5°E for the years of (a) 1998 (moderate TIW season), (b) 2001 (strongest TIW season), (c) 2006 (weakest TIW season), and (d) 2011 (moderate TIW season), with superimposed westward phase speed estimates (cf. Table 1).

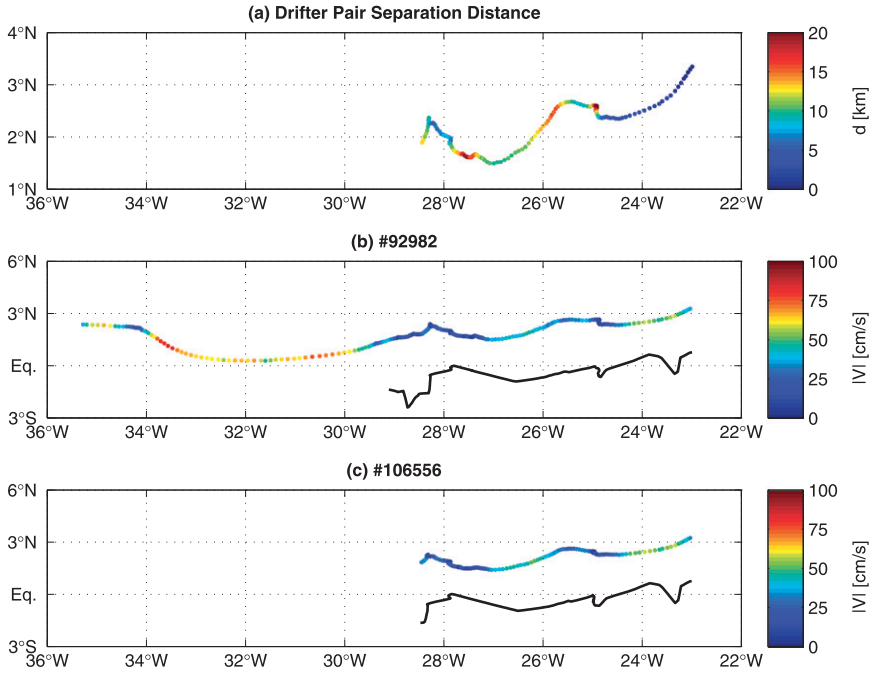

FIG. 7. (a) Position and separation distance (color) of the drifter pair deployed at 3°21.37′N, 22°59.197′W on 8 Aug 2011 (marked at mean location). (b) Position of drifter 92982 (color indicates magnitude of propagation speed) relative to the northern cold tongue front (black), with the front position given at each longitude when the drifter passed that longitude. (c) As in (b), but for drifter 106556.

range 30°W–5°E (Fig. 8b); examination of the first-crossing longitude reveals that most drifters crossed the front near the western and eastern edges of the cold tongue, where temperature gradients may be weaker (Fig. 8c). These observational results suggest that surface-constrained particles generally do not cross the equatorial cold tongue front.

The new frontal mapping methodology can reveal further aspects of the near-frontal circulation by mapping the drogued tropical Atlantic drifter velocity observations in an along- and cross-frontal frame of reference. Analysis of the flow in this reference frame complements isopycnal coordinate mapping as indicated by Perez et al. (2010) in their central equatorial Pacific study. For these analyses (Fig. 9), we utilize all available horizontal current data from the drogued drifters while the cold tongue is present, excluding observations when the front is located south of the equator (~18% of the data) to ensure comparable cases, as dynamics might be different in the Southern Hemisphere because of the change in sign of the Coriolis parameter and the proximity of the southern cold tongue front (cf. Perez et al. 2010). The drifter observations are mapped into geographic or frontal coordinates and then binned onto a regular 5° longitude × 0.5° latitude (or degrees from the front) grid using the Gaussian interpolation scheme applied earlier (influence and cutoff radii of 5° and 10° as well as 0.5° and 1°, respectively). In geographic coordinates, the zonal velocity distribution reproduces well the westward- and eastward-flowing nSEC and NECC south and north of about 3°N, respectively (Fig. 9a); when averaged in frontal coordinates, the shear zone between westward and eastward velocities is broadened (Fig. 9b). The meridional flow in geographic coordinates shows poleward velocities on both sides of the equator, indicating the expected equatorial divergence (Fig. 9d). In contrast, in frontal coordinates the flow is weakly northward across the front and there are indications of meridional convergence south of the front (Fig. 9e), which is consistent with Perez et al. (2010). As our frontal coordinate system is not truly perpendicular to the orientation of the front at any instant in time, but rather is its projection onto the meridional direction, that may result in some mean meridional flow across the front. To account for this shortcoming, we tested rotating the zonal and meridional drifter velocities in the along- and cross-frontal directions, respectively, before translating them into frontal coordinates; that is, in each instance velocities are rotated in the frontal direction using a nominal longitude range of 0.5°. While the zonal component is mostly unaffected by this rotation (Figs. 9b,c), meridional velocities are clearly increased in the rotated case, resulting in a more pronounced meridional

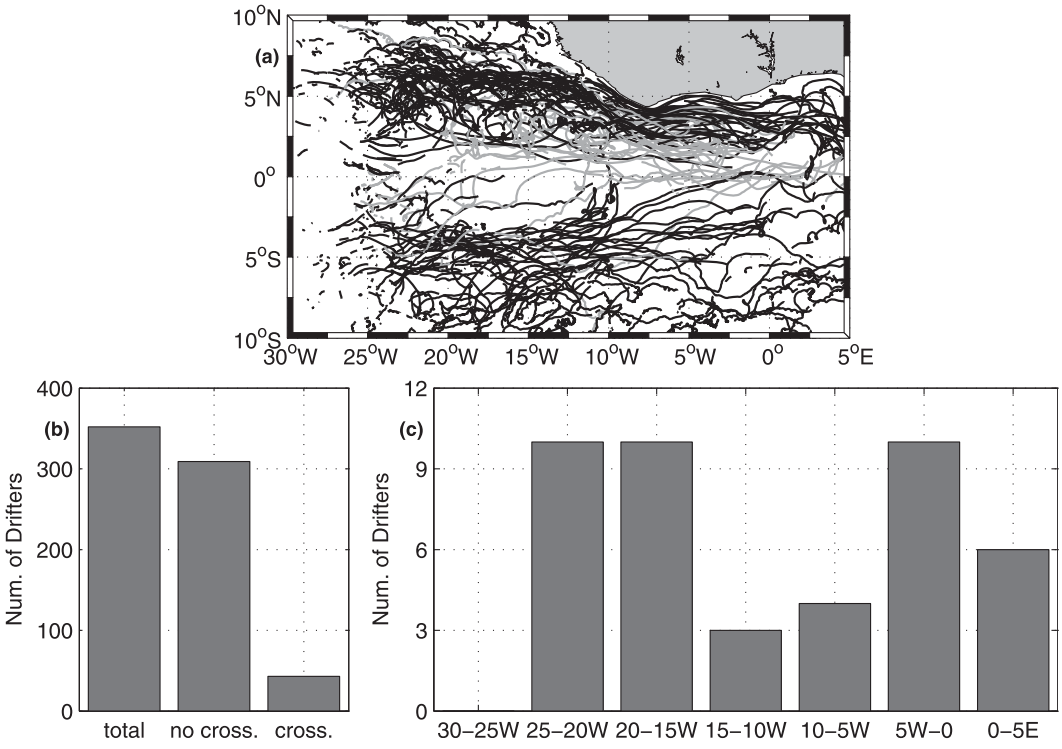

FIG. 8. (a) Trajectories of drogued tropical Atlantic drifters within the region 10°S–10°N, 30°W–5°E in the presence of the northern cold tongue front, with drifters crossing (not crossing) the front shown in gray (black), and (b) corresponding histogram. (c) Histogram of the first-crossing longitude in 5° bins.

convergence south of the front as well as a divergence north of it (Figs. 9e,f). The derived patterns may suggest that not only the meridional component but also the zonal component is of importance for frontal convergence. Using shipboard data from an intense frontal survey in the tropical Pacific, Johnson (1996) transformed the observations into a perpendicular frontal coordinate system moving with the front; assuming the surface front to be linear in form and moving steadily westward, his corresponding simple least squares fit explained more than 99% of the front's position variance. This more sophisticated analysis, however, is more readily applied to individual shipboard sections, and developing a similar methodology that can be applied across the whole zonal extent of the cold tongue and for multiple cold tongue seasons is beyond the scope of this study.

5. Discussion and conclusions

The goal of this study was to develop a generalized method for estimating the position of the Atlantic northern cold tongue front across its zonal extent more objectively than in previous cold tongue studies (Legeckis and Reverdin 1987; Steger and Carton 1991; Johnson 1996; Perez et al. 2010). Our new methodology is based on a median frontal SST criterion, and associated positional uncertainties are on the order of 0.3° latitude for the period 1998–2011. The obtained frontal characteristics are generally consistent with TIWs and interannual variations are large (Table 1).

To validate the generalized method and to demonstrate how it can be used to better understand circulation features near the northern cold tongue front, the new methodology is applied to drifter observations in the tropical Atlantic. An evaluation of the trajectories of a drifter pair deployed on the eastern side of a passing TIW crest north of the front revealed that the paths of the drifters were clearly influenced by the shape of the front and they did not cross the front, but rather stayed close together about 2.5° north of the front (Fig. 7). The sharp temperature gradient associated with the front implies that northward-moving cold water on the southern side cannot directly cross it, and the temperature distribution from PNE11-XBT data (Fig. 2a) indeed indicates a poleward tilt of the front with depth below the surface mixed layer, consistent with a slantwise motion at the front as described in the model studies by Dutrieux et al. (2008) and Perez et al. (2010). To corroborate the findings for the drifter pair, the front's permeability was further examined by applying the new methodology to the trajectories of all

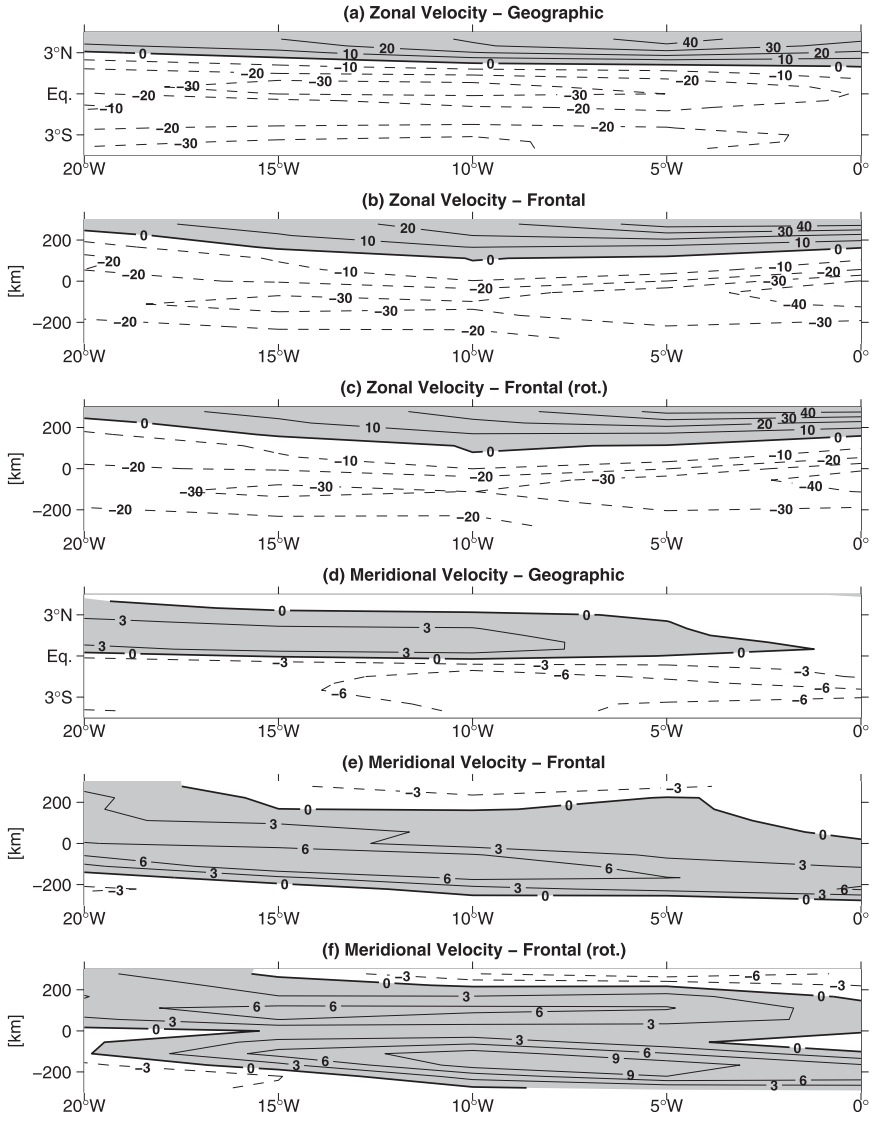

FIG. 9. Mean distribution of (a)–(c) zonal and (d)–(f) meridional velocities from drogued tropical Atlantic drifter data in (a),(d) geographic and (b),(c),(e),(f) frontal coordinates, with velocities rotated in the (c) along- and (f) cross-frontal directions.

tropical Atlantic drifters near the northern cold tongue front in the period 1998–2011 (Fig. 8); overall results suggest that surface-constrained particles generally do not cross the front. The new methodology also provided a means to analyze the tropical Atlantic drifter dataset in an along- and cross-frontal frame of reference. Our frontal analysis using available horizontal velocities from the drifters indicated a broadened nSEC–NECC shear zone as well as weak northward flow across and meridional convergence south of the northern cold tongue front when averaging in frontal coordinates (Fig. 9)—similar to the near-frontal circulation found by Perez et al. (2010) along two longitudes in the central equatorial Pacific. There are indications of stronger meridional convergence south of the front and a divergence north of it when velocities are rotated relative to the orientation of the front prior to averaging. Model studies suggest that the mean volume transport of the Atlantic shallow overturning cells known as tropical cells is diminished in the Northern Hemisphere when temporally and zonally averaged in isopycnal rather than depth coordinates (e.g., Hazeleger et al. 2003), implying that a portion of the off-equatorial downwelling may be due to averaging a quasi-adiabatic three-dimensional flow across the sloping density surfaces associated with the nonstationary equatorial cold tongue front. The generalized method developed here can serve as a complementary approach to isopycnal coordinate mapping that can be readily applied to examine

aspects of the near-frontal circulation, such as the flow associated with the tropical cells, from two-dimensional observations.

Acknowledgments. This research was carried out in part under the auspices of the Cooperative Institute for Marine and Atmospheric Studies (CIMAS), a cooperative institute of the University of Miami and the National Oceanic and Atmospheric Administration (NOAA), Cooperative Agreement NA17RJ1226. Additional support was provided by NOAA's Climate Program Office and the Atlantic Oceanographic and Meteorological Laboratory. The authors thank Chris Meinen and Jules Hummon for their help with the ADCP data as well as Erik Valdes for his help with the drifter pair observations. Comments from Sang-Ki Lee and Greg Foltz as well as three anonymous reviewers led to significant improvements in the manuscript.

REFERENCES

Brandt, P., and Coauthors, 2011: Equatorial upper-ocean dynamics and their interaction with the West African monsoon. *Atmos. Sci. Lett.,* **12,** 24–30, doi:10.1002/asl.287.

Caltabiano, A. C. V., I. S. Robinson, and L. P. Pezzi, 2005: Multi-year satellite observations of instability waves in the tropical Atlantic Ocean. *Ocean Sci.,* **1,** 97–112, doi:10.5194/os-1-97-2005.

Deans, S. R., 1983: *The Radon Transform and Some of its Applications*. John Wiley and Sons, 289 pp.

Drévillon, M., and Coauthors, 2008: The GODAE/Mercator-Ocean global ocean forecasting system: Results, applications and prospects. *J. Oper. Oceanogr.,* **1,** 51–57.

Düing, W., and Coauthors, 1975: Meanders and long waves in the equatorial Atlantic. *Nature,* **257,** 280–284, doi:10.1038/257280a0.

Dutrieux, P., C. E. Menkes, J. Vialard, P. Flament, and B. Blanke, 2008: Lagrangian study of tropical instability vortices in the Atlantic. *J. Phys. Oceanogr.,* **38,** 400–417.

Efron, B., 1987: Better bootstrap confidence intervals. *J. Amer. Stat. Assoc.,* **82,** 171–185.

Evans, W., P. G. Strutton, and F. P. Chavez, 2009: Impact of tropical instability waves on nutrient and chlorophyll distributions in the equatorial Pacific. *Deep-Sea Res. I,* **56,** 178–188, doi:10.1016/j.dsr.2008.08.008.

Foltz, G. R., S. A. Grodsky, J. A. Carton, and M. J. McPhaden, 2003: Seasonal mixed layer heat budget of the tropical Atlantic Ocean. *J. Geophys. Res.,* **108,** 3146, doi:10.1029/2002JC001584.

——, J. A. Carton, and E. P. Chassignet, 2004: Tropical instability vortices in the Atlantic Ocean. *J. Geophys. Res.,* **109,** C03029, doi:10.1029/2003JC001942.

Gentemann, C. L., F. J. Wentz, C. A. Mears, and D. K. Smith, 2004: In situ validation of Tropical Rainfall Measuring Mission microwave sea surface temperatures. *J. Geophys. Res.,* **109,** C04021, doi:10.1029/2003JC002092.

Grodsky, S. A., J. A. Carton, C. Provost, J. Servain, J. A. Lorenzzetti, and M. J. McPhaden, 2005: Tropical instability waves at 0°N, 23°W in the Atlantic: A case study using Pilot Research Moored Array in the Tropical Atlantic (PIRATA) mooring data. *J. Geophys. Res.,* **110,** C08010, doi:10.1029/2005JC002941.

Hansen, D. V., and C. A. Paul, 1984: Genesis and effects of long waves in the equatorial Pacific. *J. Geophys. Res.,* **89** (C6), 10 431–10 440.

——, and P.-M. Poulain, 1996: Quality control and interpolations of WOCE-TOGA drifter data. *J. Atmos. Oceanic Technol.,* **13,** 900–909.

Hazeleger, W., P. de Vries, and Y. Friocourt, 2003: Sources of the Equatorial Undercurrent in the Atlantic in a high-resolution ocean model. *J. Phys. Oceanogr.,* **33,** 677–693.

Jochum, M., P. Malanotte-Rizzoli, and A. Busalacchi, 2004: Tropical instability waves in the Atlantic Ocean. *Ocean Modell.,* **7,** 145–163, doi:10.1016/S1463-5003(03)00042-8.

Johnson, E. S., 1996: A convergent instability front in the central tropical Pacific. *Deep-Sea Res. II,* **43,** 753–778, doi:10.1016/0967-0645(96)00034-3.

Kennan, S. C., and P. J. Flament, 2000: Observations of a tropical instability vortex. *J. Phys. Oceanogr.,* **30,** 2277–2301.

Lee, T., G. Lagerloef, M. M. Gierach, H.-Y. Kao, S. Yueh, and K. Dohan, 2012: Aquarius reveals salinity structure of tropical instability waves. *Geophys. Res. Lett.,* **39,** L12610, doi:10.1029/2012GL052232.

Legeckis, R., and G. Reverdin, 1987: Long waves in the equatorial Atlantic Ocean during 1983. *J. Geophys. Res.,* **92** (C3), 2835–2842.

Lumpkin, R., and M. Pazos, 2007: Measuring surface currents with Surface Velocity Program drifters: The instrument, its data, and some recent results. *Lagrangian Analysis and Prediction of Coastal and Ocean Dynamics,* A. Griffa et al. Eds., Cambridge University Press, 39–67.

——, S. A. Grodsky, L. Centurioni, M.-H. Rio, J. A. Carton, and D. Lee, 2013: Removing spurious low-frequency variability in drifter velocities. *J. Atmos. Oceanic Technol.,* **30,** 353–360.

Menkes, C. E., and Coauthors, 2002: A whirling ecosystem in the equatorial Atlantic. *Geophys. Res. Lett.,* **29,** 1553, doi:10.1029/2001GL014576.

Niiler, P. P., 2001: The World Ocean surface circulation. *Ocean Circulation and Climate,* International Geophysics Series, Vol. 77, Academic Press, 193–204.

Perez, R. C., M. F. Cronin, and W. S. Kessler, 2010: Tropical cells and a secondary circulation near the northern front of the equatorial Pacific cold tongue. *J. Phys. Oceanogr.,* **40,** 2091–2106.

——, R. Lumpkin, W. E. Johns, G. R. Foltz, and V. Hormann, 2012: Interannual variations of Atlantic tropical instability waves. *J. Geophys. Res.,* **117,** C03011, doi:10.1029/2011JC007584.

Philander, S. G. H., 1978: Instabilities of zonal equatorial currents, 2. *J. Geophys. Res.,* **83** (C7), 3679–3682.

Qiao, L., and R. H. Weisberg, 1995: Tropical instability wave kinematics: Observations from the Tropical Instability Wave Experiment. *J. Geophys. Res.,* **100** (C5), 8677–8693.

Steger, J. M., and J. A. Carton, 1991: Long waves and eddies in the tropical Atlantic Ocean: 1984–1990. *J. Geophys. Res.,* **96** (C8), 15 161–15 171.

Weisberg, R. H., and T. J. Weingartner, 1988: Instability waves in the equatorial Atlantic Ocean. *J. Phys. Oceanogr.,* **18,** 1641–1657.

Wu, Q., and K. P. Bowman, 2007a: Interannual variations of tropical instability waves observed by the Tropical Rainfall Measuring Mission. *Geophys. Res. Lett.,* **34,** L09701, doi:10.1029/2007GL029719.

——, and ——, 2007b: Multiyear satellite observations of the atmospheric response to Atlantic tropical instability waves. *J. Geophys. Res.,* **112,** D19104, doi:10.1029/2007JD008627.

Zebiak, S. E., 1993: Air–sea interaction in the equatorial Atlantic region. *J. Climate,* **6,** 1567–1586.